

# Spin-state Crossover Model for the Magnetism of Iron Pnictides

Jiří Chaloupka<sup>1,2</sup> and Giniyat Khaliullin<sup>1</sup>

<sup>1</sup>Max Planck Institute for Solid State Research, Heisenbergstrasse 1, D-70569 Stuttgart, Germany

<sup>2</sup>Central European Institute of Technology, Masaryk University, Kotlářská 2, 61137 Brno, Czech Republic

(Dated: August 22, 2018)

We propose a minimal model describing magnetic behavior of Fe-based superconductors. The key ingredient of the model is a dynamical mixing of quasi-degenerate spin states of  $\text{Fe}^{2+}$  ion by intersite electron hoppings, resulting in an effective local spin  $S_{\text{eff}}$ . The moments  $S_{\text{eff}}$  tend to form singlet pairs, and may condense into a spin nematic phase due to the emergent biquadratic exchange couplings. The long-range ordered part  $m$  of  $S_{\text{eff}}$  varies widely,  $0 \leq m \leq S_{\text{eff}}$ , but magnon spectra are universal and scale with  $S_{\text{eff}}$ , resolving the puzzle of large but fluctuating Fe-moments. Unusual temperature dependences of a local moment and spin susceptibility are also explained.

PACS numbers: 75.10.Jm, 74.70.Xa, 71.27.+a

Since the discovery of superconductivity (SC) in doped  $\text{LaFeAsO}$  [1], a number of Fe-based SC's have been found and studied [2]. Evidence is mounting that quantum magnetism is an essential part of the physics of Fe-based SC's. However, the origin of magnetic moments and the mechanisms that suppress their long-range order (LRO) in favor of SC remain far from being well understood.

The magnetic behavior of Fe-based SC's is unusual. The ordered moments range from  $0.1 - 0.4 \mu_B$ , as in spin-density wave (SDW) metals like Cr, to  $1 - 2 \mu_B$  typical for Mott insulators, causing debates whether the spin-Heisenberg [3–8] or fermionic-SDW pictures [9–13] are more adequate. At the same time, irrespective to the strength or very presence of LRO, the Fe-ions possess the fluctuating moments  $\sim 1 - 2 \mu_B$  [15, S2], even in apparently “nonmagnetic”  $\text{LiFeAs}$  and  $\text{FeSe}$ . In fact, it was noticed early on that the Fe-moments, “formed independently on fermiology” [16] and “present all the time” [3], are instrumental to reproduce the measured bond-lengths and phonon spectra [3, 16–18]. Recent experiments [19–21] observe intense high-energy spin-waves that are almost independent of doping, further supporting a notion of local moments induced by Hund's coupling [22] and coexisting [23–25] with metallic bands.

While the formation of the local moments in multi-orbital systems is natural, it is puzzling that these moments (residing on a simple square lattice) may remain quantum disordered in a broad phase space despite a sizable interlayer coupling; moreover, the Fe-pnictides are semimetals with strong tendency of the electron-hole pairs to form SDW state, further *supporting* classical LRO of the underlying moments. A fragile nature of the magnetic-LRO in Fe-pnictides thus implies the presence of a strong quantum disorder effects, not captured by *ab-initio* calculations that invariably lead to magnetic order over an entire phase diagram. The ideas of domain wall motion [17] and local spin fluctuations [22] were proposed as a source of spin disorder, but no clear and tractable model of quantum magnetism in Fe-based SC's has emerged to date. Here we propose such a model.

Since Fe-pnictides are distinct among the other (Mn, Co, Ni) families, their unique physics should be rooted in specific features of the Fe-ion itself. In fact,  $\text{Fe}^{2+}$  is famous for its spin-crossover [26]: it may adopt either of  $S=0, 1, 2$  states depending on orbital splitting, covalency, and Hund's coupling. As the ionic radius of Fe is sensitive to its spin, Fe- $X$  bond length ( $X$  is a ligand) is also crucial. In oxides,  $S=2$  is typical and  $S=0, 1$  occur at high pressures only [27]. In compounds with more covalent Fe- $X$  bonds ( $X=\text{S, As, Se}$ ),  $S=0$  is more common while  $S=1, 2$  levels are higher. Here it comes the basic idea of this Letter: when the covalency and Hund's coupling effects compete, the many-body ground state (GS) is a *coherent superposition* of different spin states intermixed by electron hoppings, resulting in an *average* effective spin  $S_{\text{eff}}$  whose length depends on pressure, etc. We explore this dynamical spin-crossover idea, and find that: (i) local moment  $S_{\text{eff}}$  may *increase* with temperature explaining recent data [28]; (ii) interactions between  $S_{\text{eff}}$  contain large biquadratic exchange, and resulting spin-nematic correlations compete with magnetic-LRO; (iii) the ordered moment  $m$  varies widely, but magnon spectra are universal and scale with  $S_{\text{eff}}$  as observed [19, 20, 29]; (iv) singlet correlations among  $S_{\text{eff}}$  lead to the increase of the spin susceptibility with temperature [30].

The Fe-ions in pnictides have a formal valence state  $\text{Fe}^{2+}(d^6)$ . Among its possible spin states [Fig. 1(a)], low-spin ones are expected to be favored; otherwise, the ordered moment would be too large and robust. The  $S = 0, 1$  states, “zoomed-in” further in Fig. 1(b), are most important since they can overlap in the many-body GS by an exchange of just two electrons between ions, see Fig. 1(c). The corresponding  $\kappa$ -process converts  $\text{Fe}(S=0)\text{-Fe}(S=0)$  pair into  $\text{Fe}(S=1)\text{-Fe}(S=1)$  singlet pair and vice versa; this requires the *interorbital* hopping which is perfectly allowed for  $\sim 109^\circ$  Fe-As-Fe bonding. Basically,  $\kappa$  is a part of usual exchange process when local Hilbert space includes different spin states  $S=0, 1$ ; hence  $\kappa \sim J$ . Coupling  $J$  between  $S=1$  triplets is contributed also by their indirect interaction via the

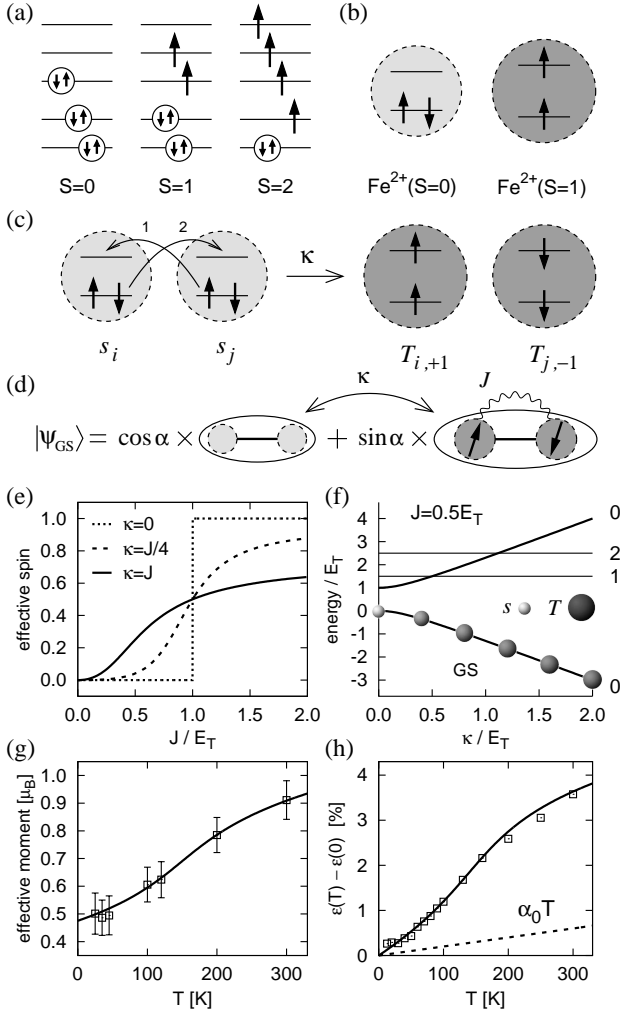


FIG. 1. (a) Schematic view of low ( $S = 0$ ), intermediate ( $S = 1$ ), and high ( $S = 2$ ) spin states of Fe<sup>2+</sup> ( $3d^6$ ). (b)  $S = 0$  and  $S = 1$  states differ in two electrons (out of six) occupying either the same or two different  $t_{2g}$  orbitals. The  $S = 1$  state has a larger ionic radius. (c) The  $\kappa$ -process generating a singlet pair of  $S = 1$  triplets  $T$  of two Fe<sup>2+</sup> ions, both originally in the  $S = 0$  state (denoted by  $s$ ). (d) The GS wavefunction of a Fe<sup>2+</sup>-Fe<sup>2+</sup> pair is a coherent superposition of two total-singlet states. (e) Effective spin (average occupation of  $S = 1$  state) depending on the ratio of the coupling  $J$  between  $S = 1$  states and their energy  $E_T$ . (f) Energy levels labeled by the total spin value of the Fe<sup>2+</sup>-Fe<sup>2+</sup> pair. Only singlet pairs are affected by  $\kappa$ . With increasing  $\kappa$ , the  $S = 1$  states are gradually mixed into the GS. (g) Temperature dependence of the local magnetic moment  $2n_T$ , and (h) the  $c$ -axis thermal expansion. Squares in (g,h) represent experimental data on Ca<sub>0.78</sub>La<sub>0.22</sub>Fe<sub>2</sub>As<sub>2</sub> [28]. Dashed line in (h) is a thermal expansion excluding magnetoelastic term.

electron-hole Stoner continuum and, as expected, it reduces with doping [31] as the electron-hole balance of a parent semimetal becomes no longer perfect.

The Hamiltonian describing the above physics comprises three terms: on-site energy  $E_T$  of  $S=1$  triplet  $T$

relative to  $S=0$  singlet  $s$ , and the bond interactions  $\kappa, J$ :

$$\mathcal{H} = E_T \sum_i n_{T_i} + \sum_{\langle ij \rangle} \left[ -\kappa_{ij} (D_{ij}^\dagger s_i s_j + \text{h.c.}) + J_{ij} \mathbf{S}_i \cdot \mathbf{S}_j \right]. \quad (1)$$

The operator  $D_{ij}^\dagger$  creates a singlet pair of spinfull  $T$ -particles on bond  $\langle ij \rangle$ . For a general spin  $S$  of  $T$ -particles,  $D_{ij} = \sum_M (-1)^{M+S} T_{i,+M} T_{j,-M}$  with  $M = -S, \dots, S$  denoting the  $N = 2S + 1$  projections; physically,  $N = 3$ . The constraint  $n_{s_i} + n_{T_i} = 1$  is implied [32, 33].

The above model rests on three specific features of Fe-pnictides/chalcogenides: (i) spin-state flexibility of Fe<sup>2+</sup> that can be tuned by pressure increasing  $E_T$ , (ii) edge-sharing FeX<sub>4</sub> tetrahedral structure allowing “spin-mixing”  $\kappa$ -term, and (iii) semimetallic nature which makes  $J$  values to decrease upon doping [31].

Figure 1(d-f) demonstrates the behavior of spin-1  $T$ -particles ( $N = 3$ ) on a single bond. The GS wavefunction  $|\psi_{\text{GS}}\rangle = \cos \alpha |A\rangle + \sin \alpha |B\rangle$  is a superposition of two singlets  $A = s_1^\dagger s_2^\dagger$  and  $B = -\frac{1}{\sqrt{3}} \sum_M (-1)^M T_{1,M}^\dagger T_{2,-M}^\dagger$ , with the “spin-mixing” angle  $\tan 2\alpha = \sqrt{3}\kappa / (E_T - J)$ . The GS energy  $E_{\text{GS}} = (E_T - J) - \sqrt{(E_T - J)^2 + 3\kappa^2}$ . At  $\kappa = 0$ , there is a sudden jump [Fig. 1(e)] from  $S = 0$  state to  $S = 1$  once the  $J$ -energy compensates the cost of having two  $T$ -particles. At finite  $\kappa$ , the dynamical mixing of spin states converts this transition into a spin-crossover, where the effective spin-length  $S_{\text{eff}} = n_T = \sin^2 \alpha$  increases gradually. Fig. 1(f) shows that  $\kappa$ -term strongly stabilizes the singlet pair of  $T$ -particles; this leads (see later) to a large biquadratic coupling  $(\mathbf{S}_1 \cdot \mathbf{S}_2)^2$  which is essential in Fe-pnictides [31, 34, 35].

We are ready to show the model in action, explaining recent observation of an unusual increase of the local moment upon warming [28]. This fact is at odds with Heisenberg and SDW pictures but easy to understand within the spin-crossover model. Indeed, the spin-length  $S_{\text{eff}}$  may vary as a function of  $E_T$  which, in turn, is sensitive to lattice expansion; in fact, Gretarsson *et al.* found that the moment value follows  $c$ -axis thermal expansion  $\epsilon = \delta c / c$ . We add (magnetoelastic) coupling  $-A\epsilon n_T$  in Eq. (1), affecting  $E_T$  value, and evaluate  $\epsilon$  and  $\langle n_T \rangle_\epsilon$  self-consistently. This is done by minimizing the elastic energy  $\frac{1}{2} K \epsilon^2 - K \alpha_0 T \epsilon + \frac{1}{4} Q \epsilon^4$  ( $\alpha_0$  is the usual thermal expansion coefficient), together with the GS energy  $E_{\text{GS}}$  given above. This results in a linear relation  $\epsilon \simeq \alpha_0 T + \frac{A}{K} \langle n_T \rangle_\epsilon$  between the magnetic moment ( $= 2n_T$ ) and lattice expansion. They both strongly increase with temperature if lattice is “soft” enough (i.e., small  $K$ ), as demonstrated in Fig. 1(g,h) by employing the parameters  $E_T - J = 160 \text{ meV}$ ,  $\kappa = 60 \text{ meV}$ ,  $A = 1.5 \text{ eV}$ ,  $K = 4.55 \text{ eV}$ ,  $Q = 250 \text{ eV}$ , and  $\alpha_0 = 0.2 \times 10^{-4} \text{ K}^{-1}$ , providing a good fit to the experimental data of Ref. [28].

Turning to collective behavior of the model, we notice first that for  $N \rightarrow \infty$  and large  $\kappa$ , the GS is dominated by tightly bound singlet dimers derived from the single-bond solution. The resonance of dimers on square-lattice

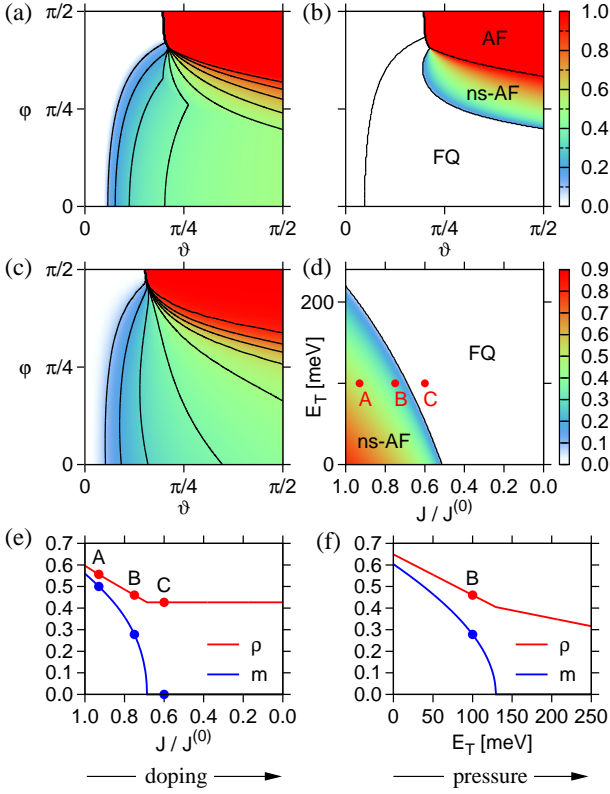


FIG. 2. (color online). (a) Condensate density  $\rho$  ( $\equiv S_{\text{eff}}$ ) obtained from Eq. (2) as a function of angles  $\vartheta, \varphi$  which parametrize the model (1) via  $E_T = \cos \vartheta$ ,  $\kappa_1 = \sin \vartheta \cos \varphi$ , and  $J_1 = \sin \vartheta \sin \varphi$ . We set  $\kappa_2/\kappa_1 = J_2/J_1 = 0.7$ . (b) The ordered spin moment value  $m$ . (c)  $T$ -occupation per site  $n_T$  obtained by an exact diagonalization of 12-site cluster, to be compared with  $\rho$  of panel (a). (d) The ordered moment  $m$  as a function of  $E_T$  and relative  $J$ -strength for fixed  $\kappa_1 = 100$  meV,  $\kappa_2 = 0.7\kappa_1$ ,  $J_1^{(0)} = 140$  meV,  $J_2^{(0)} = 0.7J_1^{(0)}$ . (e,f) Effective spin-length  $\rho = S_{\text{eff}}$  and ordered moment  $m$  at the (e)  $E_T = 100$  meV and (f)  $J/J^{(0)} = 0.75$  lines through the phase diagram in (d).

plaquettes then supports a columnar state [36] breaking lattice symmetry without magnetic LRO [33]. In the opposite limit of  $N = 1$ , the model shows a condensation of  $T$ -bosons. We found that the  $N = 3$  model relevant here is also unstable towards a condensation of  $T$ -particles with  $S = 1$ . This condensate hosts interesting properties not present in a conventional Heisenberg model. We discuss them based on the following wavefunction describing Gutzwiller-projected condensate of spin-1  $T$ -bosons:

$$|\Psi\rangle = \prod_i \left[ \sqrt{1-\rho} s_i^\dagger + \sqrt{\rho} \sum_{\alpha=x,y,z} d_{\alpha i}^* T_{\alpha i}^\dagger \right] |\text{vac}\rangle, \quad (2)$$

where  $\rho \in [0, 1]$  is the condensate density to be understood as the effective spin-length  $S_{\text{eff}}$ . The complex unit vectors  $\mathbf{d}_i = \mathbf{u}_i + i\mathbf{v}_i$  ( $u_i^2 + v_i^2 = 1$ ) determine the spin structure of the condensate in terms of the coherent states of spin-1 [37, 38] corresponding to

$T_x = (T_{+1} - T_{-1})/\sqrt{2}i$ ,  $T_y = (T_{+1} + T_{-1})/\sqrt{2}$ ,  $T_z = iT_0$ . The GS phase diagram obtained by minimizing  $\langle \Psi | \mathcal{H} | \Psi \rangle$  and cross-checked by an exact diagonalization on a small cluster is presented in Fig. 2. We have included nearest-neighbor (NN) and next-NN interactions and fixed their ratio at  $J_2/J_1 = \kappa_2/\kappa_1 = 0.7$ , reflecting large next-NN overlap via As ions. Like in  $J_1 - J_2$  model, this ratio decides between  $(\pi, \pi)$  and  $(\pi, 0)$  order. Fig. 2(a,b) contains, apart from a disordered (uncondensed) phase ( $\rho = 0$ ) at small  $\kappa, J$ , three distinct phases depending on  $\kappa/E_T$  and  $J/E_T$  values: (i) Ferroquadrupolar (FQ) phase with  $\mathbf{u}_i = \mathbf{u}$  and  $\mathbf{v}_i = 0$ . This phase has zero magnetization and is characterized by the quadrupolar order parameter  $\langle S^\alpha S^\beta - \frac{1}{3}S^2\delta_{\alpha\beta} \rangle = \rho(\frac{1}{3}\delta_{\alpha\beta} - u_\alpha u_\beta)$  with  $\mathbf{u}$  playing the role of the *director* [38]. This state, often referred to as *spin-nematic*, appears in biquadratic-exchange [37–40] and optical lattice models [41–44]. (ii) Non-saturated antiferromagnetic (ns-AF) phase with stripy magnetic order, specified by  $\mathbf{u}_i = (0, 0, u)$  and  $\mathbf{v}_i = (0, v, 0)e^{i\mathbf{Q}\cdot\mathbf{R}_i}$  with  $\mathbf{Q} = (\pi, 0)$ . The LRO-moment  $\langle \mathbf{S} \rangle$  given by  $m = 2\rho v$  can take values from 0 to  $S_{\text{eff}} = \rho$ . (iii) Saturated antiferromagnet (AF) with the same  $\mathbf{Q}$  vector, but now with  $u = v = 1/\sqrt{2}$  and  $m = S_{\text{eff}} = 1$ .

The part of the phase diagram relevant to pnictides is shown in Fig. 2(d). The decrease of  $J$  is associated with doping that changes the nesting conditions [31], while the increase of  $E_T$  is related to external/chemical pressure. Fig. 2(e,f) shows that the LRO-moment  $m$  quickly vanishes as  $J$  ( $E_T$ ) values decrease (increase); however, the spin-length  $S_{\text{eff}} = \rho$  remains almost constant ( $\sim 1/2$ ), corresponding to a fluctuating magnetic moment  $\sim 1\mu_B$ . This quantum state is driven by  $\kappa$ -process which generates the spin-1 states in a form of singlet pairs.

We consider now the excitation spectrum. It is convenient to separate fast (density) and slow (spin) fluctuations. We introduce pseudospin  $\tau = 1/2$  indicating the presence of a  $T$ -particle, and a vector field  $\mathbf{d}$  defining the spin-1 operator as  $\mathbf{S} = -i(\mathbf{d}^\dagger \times \mathbf{d})$ . The resulting Hamiltonian

$$\begin{aligned} \mathcal{H} = E_T \sum_i \left( \frac{1}{2} - \tau_i^z \right) - \sum_{\langle ij \rangle} \kappa_{ij} (\tau_i^+ \tau_j^+ \mathbf{d}_i \cdot \mathbf{d}_j + \text{h.c.}) \\ - \sum_{\langle ij \rangle} J_{ij} \left( \frac{1}{2} - \tau_i^z \right) \left( \frac{1}{2} - \tau_j^z \right) (\mathbf{d}_i^\dagger \times \mathbf{d}_i) \cdot (\mathbf{d}_j^\dagger \times \mathbf{d}_j) \end{aligned} \quad (3)$$

is decoupled on a mean-field level. The condensate spin dynamics is then given by  $O(3)$ -symmetric Hamiltonian

$$\mathcal{H}_d = - \sum_{\langle ij \rangle} \tilde{\kappa}_{ij} (\mathbf{d}_i \cdot \mathbf{d}_j + \text{h.c.}) - \sum_{\langle ij \rangle} \tilde{J}_{ij} (\mathbf{d}_i^\dagger \times \mathbf{d}_i) \cdot (\mathbf{d}_j^\dagger \times \mathbf{d}_j) \quad (4)$$

with the renormalized  $\tilde{\kappa}_{ij} = \kappa_{ij} \langle \tau_i^+ \tau_j^+ \rangle \approx \kappa_{ij}(1-\rho)\rho$  and  $\tilde{J}_{ij} \approx J_{ij}\rho^2$ . The excitations are found by introducing  $a, b, c$  bosons according to  $\mathbf{d} = (d_x, d_y, d_z) = (a, ub - iv e^{i\mathbf{Q}\cdot\mathbf{R}} c, -iv e^{i\mathbf{Q}\cdot\mathbf{R}} b + uc)$ , and replacing the condensed one as  $c, c^\dagger \rightarrow \sqrt{1-n_a - n_b}$ . The resulting

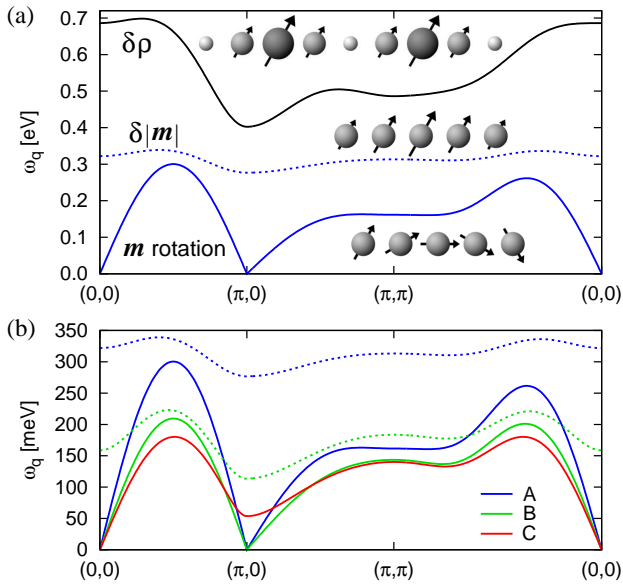


FIG. 3. (color online). (a) Dispersion of the condensate density ( $\delta\rho$ , solid-black) and the ordered moment-length ( $\delta|m|$ , dotted-blue) fluctuations, and the magnon dispersion (solid-blue), at the point A in the phase diagram of Fig. 2(d). All three modes are active in resonant x-ray scattering, and the latter two in neutron scattering. (b) Evolution of the magnetic excitations going from FQ to the ns-AF phase [ $C \rightarrow B \rightarrow A$  in Fig. 2(d)]. Two-fold degenerate quadrupole-waves (C) split into the magnon (solid lines) and the  $\delta|m|$  mode (dotted lines). The latter represents oscillations between the nematic and magnetic orderings and is gapful.

(a, b) Hamiltonian is solved by the Bogoliubov transformation. A similar approach is used for the  $\tau$ -sector describing the condensate density fluctuations  $\delta\rho = \delta S_{\text{eff}}$ .

Shown in Fig. 3 is the excitation spectra for several points of the phase diagram. The spin-length fluctuations  $\delta S_{\text{eff}}$  are high in energy. Fig. 3(b) focuses on the magnetic excitations. In the FQ phase, quadrupole/magnetic modes are degenerate and gapless at  $\mathbf{q} = 0$ . As the AF phase is approached, the gap at  $\mathbf{Q}$  decreases, and closes upon entering the magnetic phase. However, the higher energy magnons (which scale with  $S_{\text{eff}}$ ) are not much affected by transition, apart from getting (softer) harder in a (dis)ordered phase; this explains the persistence of well-defined high-energy magnons into nonmagnetic phases [19, 20].

The magnetic modes in Fig. 3(b) resemble excitations of bilinear-biquadratic spin model [38]. In fact, the dispersion in FQ phase can be *exactly* reproduced [45] from an effective spin-1 model  $\sum_{\langle ij \rangle} \tilde{J}_{ij} \mathbf{S}_i \cdot \mathbf{S}_j - \tilde{\kappa}_{ij} (\mathbf{S}_i \cdot \mathbf{S}_j)^2$ , with  $\tilde{J}$  and  $\tilde{\kappa}$  given above. A large biquadratic coupling was indeed found to account for many observations in Fe-pnictides [8, 31, 34]. We note however, that this model possesses FQ and AF phases only and misses the ns-AF phase, where the ordered moment is reduced already at the classical level; also, it does not contain the key notion

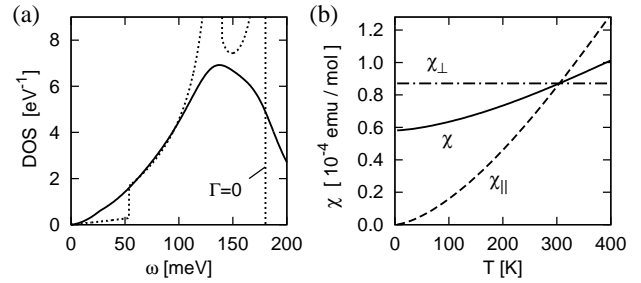


FIG. 4. (a) Density of states of the magnetic excitations calculated for the point C of Fig. 2(d). We included the damping (e.g., due to coupling to the Stoner continuum) in a form  $\Gamma(\omega) = \min(\omega, \Gamma)$  with  $\Gamma = \omega\mathbf{Q}/2$ . The result with  $\Gamma = 0$  is shown for comparison. (b) Temperature dependence of the uniform susceptibility  $\chi$ . The components  $\chi_{\parallel}$  ( $\chi_{\perp}$ ) parallel (perpendicular) to the local director  $\mathbf{u}$  are also shown.

of the original model, i.e., formation of the effective spin  $S_{\text{eff}}$  and its fluctuations.

Singlet correlations inherent to the model may also lead to increase of the paramagnetic susceptibility  $\chi(T)$  with temperature [30]. Considering nonmagnetic phase, we find that for the field parallel to the director  $\mathbf{u}$ ,  $\chi$  is temperature dependent,  $\chi_{\parallel} = \frac{1}{2T} \int d\omega \mathcal{N}(\omega) \sinh^{-2} \frac{\omega}{2T}$ , where  $\mathcal{N}(\omega) = \sum_{\mathbf{q}} \delta(\omega - \omega_{\mathbf{q}})$  is the density of states (DOS) of magnetic excitations, while  $\chi_{\perp}$  is constant. The average  $\chi = (\chi_{\parallel} + 2\chi_{\perp})/3$  (with additional factor of  $4\rho^2 \mu_B^2 N_A$ ) gives the measured  $\chi(T)$ , assuming slow rotations of the director. The DOS shown in Fig. 4(a) is contributed mainly by the regions around  $(\pi, 0)$  and  $(0, \pi)$  hosting AF correlations. The corresponding thermal excitations lead to the increase of  $\chi$  [Fig. 4(b)].

To conclude, we proposed the model describing quantum magnetism of Fe-pnictides. Their universal magnetic spectra, wide-range variations of the LRO-moments, emergent biquadratic-spin couplings are explained. The model stands also on its own: extending the Heisenberg models to the case of “mixed-spin” ions, it represents a novel many-body problem. Of a particular interest is the effect of band fermions which should have a strong impact on low energy dynamics of the model, e.g., converting the  $\mathbf{q} = 0$  Goldstone modes into overdamped spin-nematic fluctuations. Understanding the effects of coupling between local moments and band fermions, including implications for SC, should be the next step towards a complete theory of Fe-pnictides.

J.C. acknowledges support by the Alexander von Humboldt Foundation, ERDF under project CEITEC (CZ.1.05/1.1.00/02.0068) and EC 7<sup>th</sup> Framework Programme (286154/SYLICA).

[1] Y. Kamihara *et al.*, J. Am. Chem. Soc. **130**, 3296 (2008).

- [2] For a review of the experimental data, see, e.g., D.C. Johnston, *Adv. Phys.* **59**, 803 (2010).
- [3] T. Yildirim, *Physica C* **469**, 425 (2009).
- [4] C. Xu, M. Müller, and S. Sachdev, *Phys. Rev. B* **78**, 020501(R) (2008).
- [5] Q. Si and E. Abrahams, *Phys. Rev. Lett.* **101**, 076401 (2008).
- [6] C. Fang *et al.*, *Phys. Rev. B* **77**, 224509 (2008).
- [7] G. Uhrig *et al.*, *Phys. Rev. B* **79**, 092416 (2009).
- [8] D. Stanek, O.P. Sushkov, and G. Uhrig, *Phys. Rev. B* **84**, 064505 (2011).
- [9] I.I. Mazin, D.J. Singh, M.D. Johannes, and M.H. Du, *Phys. Rev. Lett.* **101**, 057003 (2008).
- [10] K. Kuroki *et al.*, *Phys. Rev. Lett.* **101**, 087004 (2008).
- [11] A.V. Chubukov, D.V. Efremov, and I. Eremin, *Phys. Rev. B* **78**, 134512 (2008).
- [12] S. Graser, T.A. Maier, P.J. Hirschfeld, and D.J. Scalapino, *New J. Phys.* **11**, 025016 (2009).
- [13] E. Kaneshita, T. Morinari, and T. Tohyama, *Phys. Rev. Lett.* **103**, 247202 (2009).
- [14] H. Gretarsson *et al.*, *Phys. Rev. B* **84**, 100509(R) (2011).
- [15] P. Vilmercati *et al.*, *Phys. Rev. B* **85**, 220503(R) (2012).
- [16] M.D. Johannes, I.I. Mazin, and D.S. Parker, *Phys. Rev. B* **82**, 024527 (2010).
- [17] I.I. Mazin and M.D. Johannes, *Nature Phys.* **5**, 141 (2009).
- [18] D. Reznik *et al.*, *Phys. Rev. B* **80**, 214534 (2009).
- [19] M. Liu *et al.*, *Nature Phys.* **8**, 376 (2012).
- [20] K.-J. Zhou *et al.*, *Nature Commun.* **4**, 1470 (2013).
- [21] M. Wang *et al.*, arXiv:1303.7339.
- [22] Z.P. Yin, K. Haule, and G. Kotliar, *Nature Mater.* **10**, 932 (2011).
- [23] J. Dai, Q. Si, J.-X. Zhu, and E. Abrahams, *Proc. Natl. Acad. Sci. U.S.A.* **106**, 4118 (2009).
- [24] S.-P. Kou, T. Li, and Z.-Y. Weng, *Europhys. Lett.* **88**, 17010 (2009).
- [25] W. Lv, F. Krüger, and P. Phillips, *Phys. Rev. B* **82**, 045125 (2010).
- [26] P. Gütlich and H.A. Goodwin (Eds.), *Spin Crossover in Transition Metal Compounds I* (Springer, Berlin, 2004).
- [27] S. Stackhouse, *Nature Geosci.* **1**, 648 (2008).
- [28] H. Gretarsson *et al.*, *Phys. Rev. Lett.* **110**, 047003 (2013).
- [29] J.T. Park *et al.*, *Phys. Rev. B* **86**, 024437 (2012).
- [30] R. Klingeler *et al.*, *Phys. Rev. B* **81**, 024506 (2010).
- [31] A.N. Yaresko, G.-Q. Liu, V.N. Antonov, and O.K. Andersen, *Phys. Rev. B* **79**, 144421 (2009).
- [32] In the Supplemental Material, we derive the Hamiltonian (1) from a two-orbital Hubbard model.
- [33] To address a tetra/ortho structural ("orbital order") transition, we may include also  $xz/yz$  orbital degeneracy of  $S = 1$  triplets; this is left for future work.
- [34] A.L. Wysocki, K.D. Belashchenko, and V.P. Antropov, *Nature Phys.* **7**, 485 (2011).
- [35] R. Yu *et al.*, *Phys. Rev. B* **86**, 085148 (2012).
- [36] N. Read and S. Sachdev, *Phys. Rev. Lett.* **62**, 1694 (1989).
- [37] B.A. Ivanov and A.K. Kolezhuk, *Phys. Rev. B* **68**, 052401 (2003).
- [38] A. Läuchli, F. Mila, and K. Penc, *Phys. Rev. Lett.* **97**, 087205 (2006).
- [39] H. Tsunetsugu and M. Arikawa, *J. Phys. Soc. Jpn.* **75**, 083701 (2006).
- [40] K. Harada and N. Kawashima, *Phys. Rev. B* **65**, 052403 (2002).
- [41] E. Demler and F. Zhou, *Phys. Rev. Lett.* **88**, 163001 (2002); A. Imambekov, M. Lukin, and E. Demler, *Phys. Rev. B* **68**, 063602 (2003).
- [42] S.K. Yip, *Phys. Rev. Lett.* **90**, 250402 (2003).
- [43] C.M. Puetter, M.J. Lawler, and H.-Y. Kee, *Phys. Rev. B* **78**, 165121 (2008).
- [44] M. Serbyn, T. Senthil, and P.A. Lee, *Phys. Rev. B* **84**, 180403(R) (2011).
- [45] This can be understood using the identity  $(\mathbf{S}_i \cdot \mathbf{S}_j)^2 = |\mathbf{d}_i \cdot \mathbf{d}_j|^2 + 1$ . If  $v \ll u \approx 1$ , like in the FQ phase or close to it in the ns-AF phase, we recover the  $\kappa$ -term of Eq. (4):  $(\mathbf{S}_i \cdot \mathbf{S}_j)^2 \approx \mathbf{d}_i \cdot \mathbf{d}_j + \mathbf{d}_i^\dagger \cdot \mathbf{d}_j^\dagger$ .

Supplemental Material for

## Spin-state crossover model for the magnetism of iron pnictides

Jiří Chaloupka<sup>1,2</sup> and Giniyat Khaliullin<sup>1</sup>

<sup>1</sup> *Max Planck Institute for Solid State Research, Heisenbergstrasse 1, D-70569 Stuttgart, Germany*

<sup>2</sup> *Central European Institute of Technology, Masaryk University, Kotlářská 2, 61137 Brno, Czech Republic*

Here we analyze two-orbital Hubbard model in the regime of large Hund's coupling and large interorbital hopping, and explicitly demonstrate the emergence of the effective model proposed in the main paper. We also provide estimates of the model parameters in terms of the microscopic parameters of the Hubbard model.

Based on the "orbital-differentiation" mechanism – which is particularly pronounced in multiorbital systems with large Hund's coupling (see Ref. [S1] for recent discussion) – we assume a coexistence of strongly correlated orbitals (hosting magnetic moments) and more itinerant bands (responsible for the charge transport and Fermi-surface related physics). For the Fe-pnictide/chalcogenide families, a minimal model for the "magnetic" sector is a two-orbital Hubbard model which may accommodate magnetic moments ranging from zero to  $2 \mu_B$  per Fe-ion, depending on the parameter regime. This possible moment-window is what observed in Fe-pnictide/chalcogenides [S2] (and also consistent with the model of the main text). We assume that these two orbitals (labeled  $a$  and  $b$  below) are populated by two electrons per site on average, while the remaining four electrons out of Fe- $d^6$  configuration form a semimetallic band structure. The itinerant bands are not a prime source of magnetic moments but, as noticed in the main text, we keep in mind that they may mediate the interactions between local moments and hence support their long-range order [S3, S4].

Let us focus now on the "magnetic" sector, i.e. two-orbital Hubbard Hamiltonian. As usual, it comprises two parts, local interactions and intersite hoppings:  $\mathcal{H} = \mathcal{H}_{\text{loc}} + \mathcal{H}_{\text{kin}}$ . Its local part includes the crystal field splitting  $\Delta$  between  $a$  and  $b$  orbitals (their precise structure in terms of original  $d$  states is not essential here) and local correlations:

$$\mathcal{H}_{\text{loc}} = \frac{\Delta}{2} \sum_i (n_{ib} - n_{ia}) + U \sum_{i,\gamma=a,b} n_{i\gamma\uparrow} n_{i\gamma\downarrow} + \sum_i \left[ U' - J_H \left( 2\mathbf{S}_{ia} \cdot \mathbf{S}_{ib} + \frac{1}{2} \right) \right] n_{ia} n_{ib}. \quad (\text{S1})$$

The local pair-hopping term is neglected, and the relation  $U' = U - 2J_H$  between inter- and intra-orbital Coulomb interactions will be used. The kinetic term  $\mathcal{H}_{\text{kin}}$  of the Hamiltonian contains the intersite hopping of both intra- and inter-orbital character

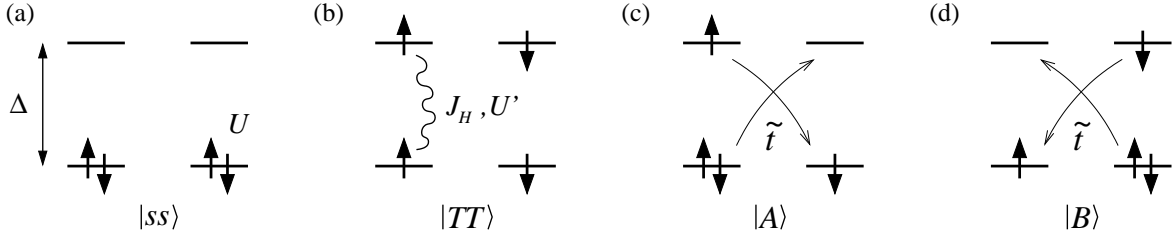
$$\mathcal{H}_{\text{kin}} = -t \sum_{\langle ij \rangle, \sigma} \left( a_{i\sigma}^\dagger a_{j\sigma} + b_{i\sigma}^\dagger b_{j\sigma} + \text{h.c.} \right) - \tilde{t} \sum_{\langle ij \rangle, \sigma} \left( a_{i\sigma}^\dagger b_{j\sigma} + b_{i\sigma}^\dagger a_{j\sigma} + \text{h.c.} \right). \quad (\text{S2})$$

Similar model was recently considered in Ref. [S5] to address the spin-transition physics in cobaltates. The key difference of our model is the presence of interorbital hopping  $\tilde{t}$ , which converts the transitions found in Ref. [S5] into a smooth spin-crossover such that the ground state magnetic moment length (not long-range order parameter!) may acquire any value from zero to  $2 \mu_B$ .

Our aim is to obtain the model Hamiltonian of the main paper as an effective low-energy Hamiltonian resulting from  $\mathcal{H} = \mathcal{H}_{\text{loc}} + \mathcal{H}_{\text{kin}}$  in the appropriate regime of parameters  $\Delta, J_H$ , etc. This is achieved by a standard procedure – we select the relevant  $d_i^2 - d_j^2$  bond states from the eigenbasis of  $\mathcal{H}_{\text{loc}}$  and obtain effective interactions on the bonds by eliminating  $\mathcal{H}_{\text{kin}}$  perturbatively, employing the low-energy  $d_i^3 - d_j^1$  and  $d_i^1 - d_j^3$  configurations as the intermediate states. To check the validity of this approach, the exact eigenstates of  $\mathcal{H}$  on a single bond are calculated and the results compared with those of the effective Hamiltonian  $\mathcal{H}_{\text{eff}}$  we have derived.

In the spin-crossover regime discussed in the main paper, large Hund's coupling nearly compensates the crystal field splitting (i.e.,  $\Delta \sim 3J_H$ ) and makes the on-site singlet  $|s\rangle = a_\uparrow^\dagger a_\downarrow^\dagger | \rangle$  and the three triplet states  $|T_{+1}\rangle = a_\uparrow^\dagger b_\uparrow^\dagger | \rangle$ ,  $|T_0\rangle = \frac{1}{\sqrt{2}}(a_\uparrow^\dagger b_\downarrow^\dagger + a_\downarrow^\dagger b_\uparrow^\dagger) | \rangle$ , and  $|T_{-1}\rangle = a_\downarrow^\dagger b_\downarrow^\dagger | \rangle$  quasidegenerate. These states thus form the relevant low-energy sector while the other states (such as  $a_\uparrow^\dagger b_\downarrow^\dagger | \rangle$ ) are much higher in energy and can be ignored.

To be able to extract the effective Hamiltonian on a bond, it is convenient to consider the subspaces with total spin  $S_{\text{tot}} = 0, 1, 2$  separately. In  $S_{\text{tot}} = 0$  sector, the relevant bond states are the two  $d_i^2 - d_j^2$  configurations depicted in Fig. S1(a, b):  $|ss\rangle = |s\rangle_i |s\rangle_j$  with the local energy  $E_{ss} = 2U - 2\Delta$ , and  $|TT\rangle = \frac{1}{\sqrt{3}} \left( |T_{+1}\rangle_i |T_{-1}\rangle_j - |T_0\rangle_i |T_0\rangle_j + |T_{-1}\rangle_i |T_{+1}\rangle_j \right)$  with the local energy  $E_{TT} = E_{ss} + 2(\Delta - 3J_H)$ . The bond interaction originates from virtual processes employing as the intermediate states mainly the low-lying  $d_i^3 - d_j^1$  and  $d_i^1 - d_j^3$  configurations presented in Fig. S1(c, d).



They are denoted as  $|A\rangle$  and  $|B\rangle$  and their local energy amounts to  $E_A = E_B = E_{ss} + U' + \Delta - 3J_H$ . The other bond states have a negligible contribution to the groundstate, due to their high energy or due to kinematic (no hopping) reasons. The lowest state in the  $S_{\text{tot}} = 1$  sector is composed of a pair of on-site triplets  $|T\rangle$  and states analogous to  $|A\rangle$  and  $|B\rangle$  but having total spin one. Finally, the only states in the  $S_{\text{tot}} = 2$  are the combinations of two on-site triplets. These states are unaffected by hopping.

The validity of the above classification of low-energy levels of Hubbard model is demonstrated in Fig. S2 showing the results of an exact diagonalization of full two-orbital model  $\mathcal{H}$  on a single bond. We consider a representative set of parameters  $\Delta$  and  $J_H$  such that a spin-crossover regime, where the on-site singlet and triplet states are quasidegenerate, is realized:  $\Delta - 3J_H = 0.1$  eV. Focusing on  $S_{\text{tot}} = 0$  sector in Fig. S2(b), we can observe that with increasing  $\tilde{t}$ , the state  $|TT\rangle$  gets gradually involved into the groundstate, which becomes a mixture of  $|ss\rangle$ ,  $|TT\rangle$  and the higher energy states  $|A\rangle$ ,  $|B\rangle$  serving as the intermediate states for the  $\kappa$ -processes. The contribution of the other states, which are neglected in our derivation of the effective Hamiltonian below, is indeed negligible.

Having selected our basis states and evaluated their local energy, we proceed now by incorporating the intersite hopping within this basis. First, the initial Hamiltonian  $\mathcal{H}$  is projected to the selected subspace of total spin  $S_{\text{tot}}$  and denoted accordingly as  $\mathcal{H}^{(S)}$  (where  $S = 0, 1, 2$ ). In the next step, the intermediate states are eliminated from  $\mathcal{H}^{(S)}$ -matrix by perturbation theory. After these steps, we will obtain an effective Hamiltonian  $\mathcal{H}_{\text{eff}}^{(S)}$  that operates

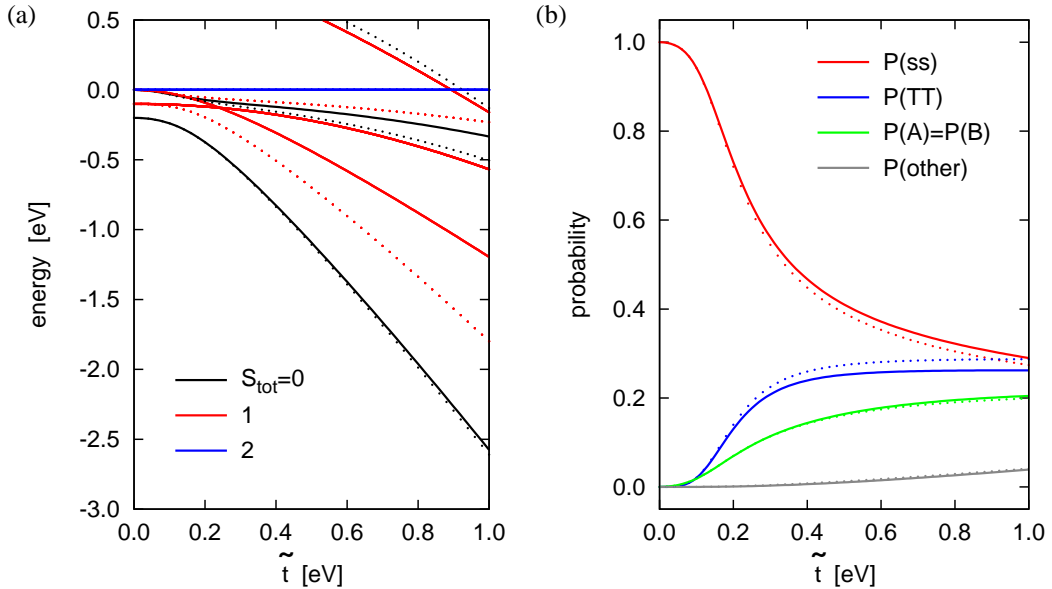


FIG. S2. (a) Exact energy levels on the bond as a function of interorbital hopping  $\tilde{t}$  for  $U = 3\text{eV}$ ,  $J_H = 1\text{eV}$ ,  $\Delta - 3J_H = 0.1\text{eV}$ , and  $t = 0$  (solid lines) and  $t = 0.5\tilde{t}$  (dotted lines). States with different values of the total spin are distinguished by color. (b) Probabilities of selected basis states  $|ss\rangle$ ,  $|TT\rangle$ ,  $|A\rangle$ , and  $|B\rangle$  in the groundstate. The other states ignored in the effective model derivation have a negligible total weight [see corresponding  $P(\text{other})$  curve]. For a moderate value of  $t$ , the energy and the composition of the groundstate remains practically unaffected.



within  $d_i^2 - d_j^2$  configuration alone, and compare it with the model Hamiltonian  $\mathcal{H}_{\text{model}}$  used in the main paper.

In the most interesting  $S_{\text{tot}} = 0$  subspace, after the elimination of intermediate states, the Hamiltonian  $\mathcal{H}$  projected to the subspace spanned by  $|ss\rangle$ ,  $|TT\rangle$ ,  $|A\rangle$ ,  $|B\rangle$  states

$$\mathcal{H}^{(0)} = \begin{pmatrix} E_{ss} & 0 & -\sqrt{2}\tilde{t} & -\sqrt{2}\tilde{t} \\ 0 & E_{TT} & -\sqrt{\frac{3}{2}}\tilde{t} & -\sqrt{\frac{3}{2}}\tilde{t} \\ -\sqrt{2}\tilde{t} & -\sqrt{\frac{3}{2}}\tilde{t} & E_A & 0 \\ -\sqrt{2}\tilde{t} & -\sqrt{\frac{3}{2}}\tilde{t} & 0 & E_B \end{pmatrix} \quad \text{becomes} \quad \mathcal{H}_{\text{eff}}^{(0)} = \begin{pmatrix} E_{ss} - \frac{4\tilde{t}^2}{\varepsilon} & -\frac{2\sqrt{3}\tilde{t}^2}{\varepsilon} \\ -\frac{2\sqrt{3}\tilde{t}^2}{\varepsilon} & E_{TT} - \frac{3\tilde{t}^2}{\varepsilon} \end{pmatrix} \quad (\text{S3})$$

operating now within the  $|ss\rangle$  and  $|TT\rangle$  singlet states of  $d_i^2 - d_j^2$  configuration. Here,  $\varepsilon = E_A - E = E_B - E$  denotes the excitation energy. In the second order perturbation theory  $E = E_{ss}$ , but by diagonalizing the energy dependent  $\mathcal{H}_{\text{eff}}^{(0)}$  self-consistently, one can exactly reproduce the groundstate energy and the ratio of  $|ss\rangle$  and  $|TT\rangle$  coefficients obtained by diagonalizing the original matrix  $\mathcal{H}^{(0)}$ . In the following, we therefore take  $E = E_{\text{GS}}$  with  $E_{\text{GS}}$  being the groundstate energy of  $\mathcal{H}_{\text{eff}}^{(0)}$ .

Using the same procedure, the pairs of local triplets  $T$  of total spin  $S_{\text{tot}} = 1$  obtain an energy  $\mathcal{H}_{\text{eff}}^{(1)} = E_1 = E_{TT} - 2\tilde{t}^2/\varepsilon'$  with  $\varepsilon' = E_A - E_1$  being the excitation energy, and those of total spin  $S_{\text{tot}} = 2$  remain at an energy  $\mathcal{H}_{\text{eff}}^{(2)} = E_{TT}$ .

The effective Hamiltonian  $\mathcal{H}_{\text{eff}}$  can now be exactly mapped to the model Hamiltonian  $\mathcal{H}_{\text{model}}$  proposed in the main paper. For a single bond, using the same notations, the corresponding matrix elements of  $\mathcal{H}_{\text{model}}$  read as

$$\mathcal{H}_{\text{model}}^{(0)} = \begin{pmatrix} 0 & -\sqrt{3}\kappa \\ -\sqrt{3}\kappa & 2E_T - 2J - 4K \end{pmatrix}, \quad \mathcal{H}_{\text{model}}^{(1)} = 2E_T - J - K, \quad \mathcal{H}_{\text{model}}^{(2)} = 2E_T + J - K. \quad (\text{S4})$$

To make the correspondence between  $\mathcal{H}_{\text{eff}}$  and  $\mathcal{H}_{\text{model}}$  matrices complete, we had to include small biquadratic exchange  $-K(\mathbf{S}_1 \cdot \mathbf{S}_2)^2$ . The term-by-term comparison of the matrix elements of  $\mathcal{H}_{\text{eff}}^{(S)}$  and  $\mathcal{H}_{\text{model}}^{(S)}$  yields the following values of the model parameters

$$\kappa = \frac{2\tilde{t}^2}{\varepsilon}, \quad J = \frac{\tilde{t}^2}{\varepsilon'}, \quad K = \tilde{t}^2 \left( \frac{1}{\varepsilon} - \frac{1}{\varepsilon'} \right), \quad E_T = (\Delta - 3J_H) + \tilde{t}^2 \left( \frac{5}{2\varepsilon} - \frac{1}{\varepsilon'} \right). \quad (\text{S5})$$

As evidenced by Fig. S3(a), the effective model gives an adequate description of the lowest states of the Hubbard model. The obtained model parameters entering Eqs. (S4) and (S5) are presented in Fig. S3(b) as functions of the interorbital hopping amplitude  $\tilde{t}$ . The realistic range of  $E_T \approx 0.1 - 0.2$  eV and  $\kappa, J \approx 0.05 - 0.20$  eV is obtained by taking  $\tilde{t} \approx 0.2 - 0.4$  eV. The small biquadratic exchange contained in  $\mathcal{H}_{\text{eff}}$  can be neglected at this point because the much larger effective biquadratic contribution is in fact generated by the  $\kappa$ -processes dynamically (see main text).

It is worth noticing that the strength  $\kappa$  of the key process of the model is finite due to interorbital hopping  $\tilde{t}$ . This process is thus ineffective in perovskite lattices, but it is perfectly allowed for the Fe-(As/Te)-Fe bonding geometry of Fe-pnictides/chalcogenides and leads to the spin-crossover mechanism ("soft" magnetism) in these compounds (see main text). Concerning the role of intra-orbital  $t$ -hopping in the mapping, it did not enter the above formulas, since  $t$  does not connect any pair of the selected low energy states. The intermediate states that can be reached by  $t$  have an energy higher by  $\Delta$  than those involved by  $\tilde{t}$ , so that the  $t$ -effect on  $\kappa$  and  $E_T$  values is relatively weak. It is only found to increase  $J$  by about  $2t^2/(\Delta + E_A - E_{TT})$ .

To conclude, we have shown that the model Hamiltonian proposed in the paper naturally emerges from the two-orbital Hubbard model with strong Hund's coupling, when a regime of spin-state quasidegeneracy is realized. The model parameters that follow from this derivation are well within the ranges that we have explored in our study.

---

[S1] A. Georges, L. de' Medici, and J. Mravlje, arXiv:1207.3033.

[S2] H. Gretarsson *et al.*, Phys. Rev. B **84**, 100509(R) (2011).

[S3] M.D. Johannes, I.I. Mazin, and D.S. Parker, Phys. Rev. B **82**, 024527 (2010).

[S4] M.D. Johannes and I.I. Mazin, Phys. Rev. B **79**, 220510(R) (2009).

[S5] J. Kuneš and V. Krápek, Phys. Rev. Lett. **106**, 256401 (2011).



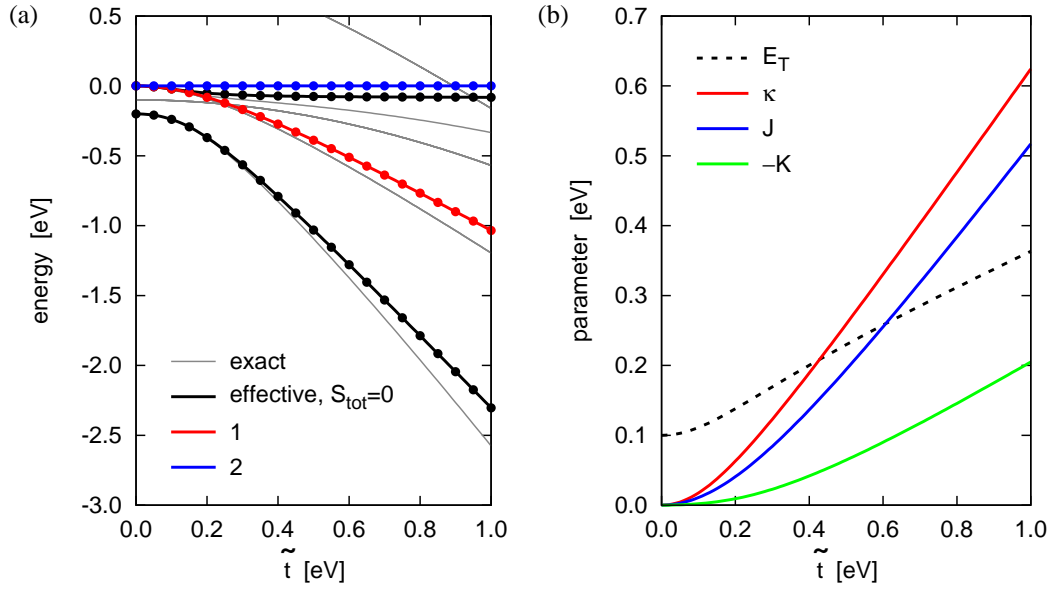


FIG. S3. (a) Energy levels resulting from the diagonalization of  $\mathcal{H}_{\text{eff}}$  compared to the exact levels of the original Hubbard Hamiltonian. The same parameters as in Fig. S2 are used and  $t = 0$ . (b) Values of the effective model parameters as functions of interorbital hopping  $\tilde{t}$ .